https://doi.org/10.5194/egusphere-2026-2154
Preprint. Discussion started: 23 April 2026

Multi-proxy evidence for orbital-paced ISM variability in PT2 lacustrine sediment records from Southwest China

Ziyi Yang[1], Xinwen Xu[1,2], Shuheng Li[1], Xiaoke Qiang[2], Le Li[1], Jingfang Zhang[1]

[1] Shaanxi Key Laboratory of Earth Surface System and Environmental Carrying Capacity, College of Urban and Environmental Science, Northwest University, Xi′an 710127, China
[2] State Key Laboratory of Loess Science, Institute of Earth Environment, Chinese Academy of Sciences, Xi′an 710061, China

Correspondence to: Xinwen Xu (xuxinwen@nwu.edu.cn); Shuheng Li (lish@nwu.edu.cn)

Abstract. The Indian summer monsoon (ISM) is strongly influenced by orbital forcing. However, the dominant cycles are different in various paleoclimate indicators. This has limited our understanding of the dynamics of the ISM. Here we present a high-resolution ISM record spanning ~184-25 ka by magnetic parameters (ARM, χ, SIRM, and χfd%) and geochemical indicators (Rb/Sr and Ti) from lacustrine sediments in the Heqing Basin, southwestern China. In the PT2 core, ARM shows the clearest precession-scale (~20 ka) variability, likely reflecting its strong sensitivity to precipitation-driven changes in fine magnetic particle input. In contrast, Rb/Sr is dominated by glacial-interglacial (~100 ka) variability, probably because it responds to slower catchment-scale processes, such as chemical weathering and sediment redistribution. During MIS 5, low detrital input and a relative enrichment of fine magnetic grains likely shifted ARM toward stronger grain-size control rather than concentration control. This may have allowed the precession-scale signal to be expressed more clearly. Reductive dissolution likely modulated the amplitude of magnetic parameters, but did not fundamentally erase their primary orbital-scale signals. Our results highlight the importance of proxy-specific interpretation and demonstrate the value of ARM for reconstructing precession-paced ISM variability in southwestern China.

1 Introduction

The Indian Summer Monsoon (ISM) is one of the most critical ocean-atmosphere circulation systems (An et al., 2011; Kathayat et al., 2016). By seasonally transporting large amounts of moisture and heat from the Indian Ocean, the ISM governs rainfall over the Indian subcontinent, much of Southeast Asia, and southern China, including southwest China and the southeastern Tibetan Plateau, and also modulates conditions over the adjacent Arabian Sea and Bay of Bengal (Wang et al., 2021). Dynamically, the monsoon is driven primarily by the land-sea thermal contrast and is modulated by the position of the westerlies and by latitudinal insolation gradients (Li et al., 2017; Zhang et al., 2025). These controls are influenced by orbital forcing (precession, obliquity, and eccentricity), which modulates the seasonal and latitudinal distribution of insolation (Berger, 1978; Milankovitch, 1941). Precession (23 ka and 19 ka, often merged into a single peak near ~20 ka) primarily drive climate variability at low latitudes (Li et al., 2024; Wu et al., 2025). In contrast, the ~41 ka obliquity cycle

https://doi.org/10.5194/egusphere-2026-2154
Preprint. Discussion started: 23 April 2026

has a stronger influence on high-latitude climate. By changing Earth's axial tilt, obliquity affects the amplitude of seasonal temperature contrasts and polar insolation, thereby favoring conditions for ice-sheet growth or retreat through feedbacks involving albedo, sea level and greenhouse gases (Bajo et al., 2020). The ~100-ka eccentricity band has only a weak direct effect on insolation and therefore the prominent ~100-ka signal in geological records largely reflects internal climate feedbacks associated with glacial-interglacial ice-volume changes (Laskar et al., 2004; Van Peer et al., 2024). Ice-sheet growth and retreat then influence global climate indirectly by changing surface albedo, altering atmospheric CO2 concentrations, adjusting sea level, and modifying large-scale temperature gradients (Van Peer et al., 2024).

Within the ISM influence zone, SW China's lake and stalagmite archives offer good records of monsoon change, and are therefore well suited for examining ISM dynamics (An et al., 2011; Cai et al., 2015; Sandeep et al., 2017; Xu et al., 2024; Zhang et al., 2023). However, climate proxies may respond differently to orbital forcing, as demonstrated by multiple lines of evidence from southwest China (An et al., 2011; Zhang et al., 2023; Xu et al., 2025). For example, Sr/Ca and Mg/Ca ratios from the Pleistocene Heqing paleolake sediments record glacial-interglacial ISM cycles within the lake's lifecycle (Yang et al., 2024). Pollen records from the same basin indicate that the regional climate and ISM variability are influenced by both the ~100 ka cycle and other major orbital and sub-orbital cycles, including ~400 ka, obliquity (41 ka and 29 ka cycles), 23 ka precession, and ~10 ka cycles (Xiao et al., 2010). In contrast, the $\delta^{18}O$ record from the Zada Basin in southwestern Tibet exhibits cycles of ~100 ka and ~20 ka. However, its high-frequency environmental variations are primarily driven by solar radiation (dominated by precession and modulated by eccentricity), rather than directly by global ice volume changes (Saadeh et al., 2020). Speleothem $\delta^{18}O$ records from Bittoo cave, Northern India, also suggest that the ISM may be driven by precession-induced Northern Hemisphere summer insolation (NHSI) changes (Kathayat et al., 2016).

In addition, regional comparison studies frequently rely on varying indicators. $\delta^{18}O$ values are widely used in paleoclimate reconstruction because they are often negatively correlated with regional precipitation (Cheng et al., 2016; Zhang et al., 2025). However, they can also be influenced by moisture source, seasonal and trajectory changes in moisture transport, and the amount effect (Li et al., 2019). Pollen proxies are susceptible to basin-scale vegetation succession, human activities, and land-use changes, which may obscure or alter climate-driven vegetation signals (Hicks, 2006; Li et al., 2014). Geochemical indicators such as the Chemical Index of Alteration (CIA) and Rb/Sr ratios are affected by basin weathering-erosion processes, runoff variations, and lake sedimentary dynamics, reflecting the integrated weathering history of the basin (Guo et al., 2018; Li and Yang, 2010; Jin et al., 2020). As crucial indicators for recording paleoclimate changes in lake sediments, magnetic proxies such as ARM exhibit marked sensitivity to orbital-scale variability and reliably record the signatures of precession, obliquity, and eccentricity (Huang et al., 2015; Li et al., 2024; Su et al., 2019). However, their interpretation can be ambiguous due to influences from redox processes and local environmental factors (Liu et al., 2012; Roberts, 2015). Climate proxies often register signals in distinct ways, relying on a single indicator can lead to biased or incomplete reconstructions. Therefore, we present magnetic and geochemical high-resolution records from lacustrine sediments in the Heqing Basin spanning ~184-25 ka. This study aims to explore the orbital periodicity of the ISM using a multi-proxy

https://doi.org/10.5194/egusphere-2026-2154
Preprint. Discussion started: 23 April 2026

approach, examining the differences in responses across various orbital scales among different proxies and the underlying reasons.

2 Study areas and methods

2.1 Study areas

The Heqing Basin is located in southwest China, on the southeastern margin of the Tibetan Plateau (Fig. 1). It is situated at the intersection of the northward extension of the Red River Fault and the Jinsha River Fault, within the Hengduan Mountains of northwestern Yunnan. The basin has an average elevation ranging from 2193 to 2240 meters above sea level (Fang et al., 2007). The climate of the Heqing Basin is strongly influenced by ISM, with summer precipitation accounting for over 80% of the annual rainfall.

The Pengtun section is located in Pengtun Village, Caohai Town, Heqing County. In 2009, a 33.9-meter-long sediment core (PT2) was extracted from the Pengtun No. 2 core (26°35′24.0″N, 100°11′08.2″E, 2188 m), located 2 kilometers from Heqing County. The core PT2 has been stored at the Core Repository of Continental Environmental Science, Institute of Earth Environment, Chinese Academy of Sciences. The lithology of the borehole primarily consists of laminated greyish-green and greyish-yellow calcareous clays and silty clays.

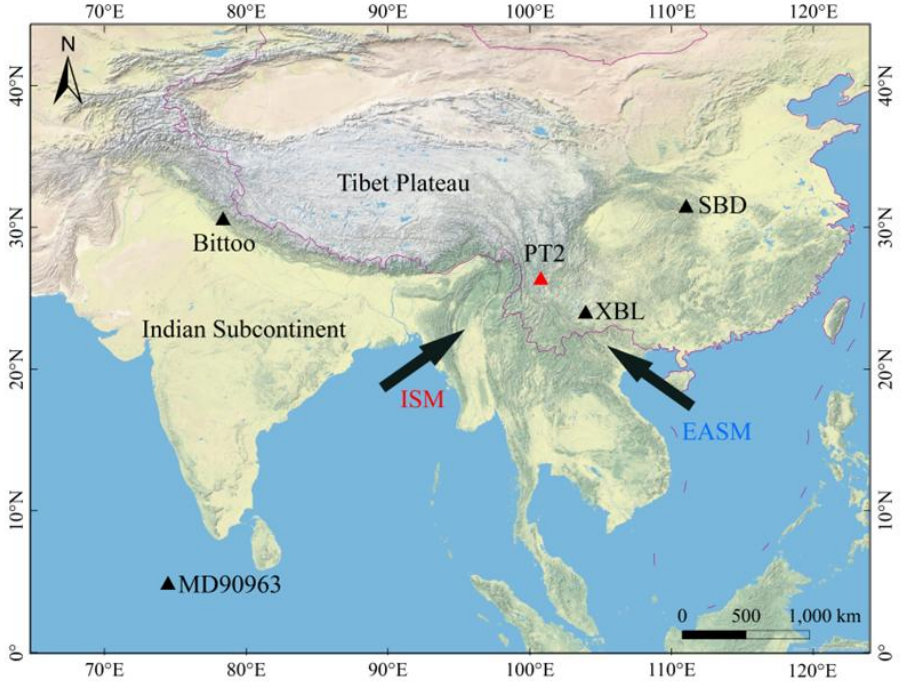

Figure 1: Location of the PT2 drill core (red triangle) in southwestern China. The sites mentioned in the text, such as Bittoo, Sanbao, and Xiaobailong caves and marine sediments (core MD90963) from the Indian Ocean, are shown as black triangles.

https://doi.org/10.5194/egusphere-2026-2154
Preprint. Discussion started: 23 April 2026

2.2 Environmental magnetism experiments

Approximately 10 g of bulk sample was dried at 35 °C, then magnetic susceptibility was measured at low (470 Hz) and high (4700 Hz) frequencies using a Bartington MS2 magnetic susceptibility instrument. After normalizing by mass, yielded low-frequency (χlf) and high-frequency (χhf) magnetic susceptibility. χ, denoting low-frequency magnetic susceptibility, is commonly used to indicate the concentration of ferrimagnetic minerals. The frequency-dependent susceptibility (χfd%, χfd%= 100% × (χlf - χhf)/ χlf) can be used to show the absolute concentration of superparamagnetic particles (SP). Anhysteretic Remanent Magnetization (ARM) and Isothermal Remanent Magnetization (IRM) were measured using the 2G-755R. ARM was obtained under a constant direct current (DC) field of 0.05 mT and an alternating field (peak field of 80 mT). The Saturated Isothermal Remanent Magnetization (SIRM) was imparted at a magnetic field of 1 T. ARM is sensitive to single-domain (SD) grains and finer vortex-state particles, and the ARM/SIRM ratio can reflect grain size (Liu et al., 2012; Zhang et al., 2019).

Based on the peaks and troughs of the χ curves, 22 samples were selected for detailed rock magnetic measurements. Temperature-dependent magnetic susceptibility (χ-T) was measured using an MFK1FA Kappabridge in an argon atmosphere. A CS-3 high-temperature furnace was used for heating over a temperature range of 40°C to 700°C. Different magnetic components display characteristic responses on the χ-T curves, allowing them to be identified. First-order reversal curves (FORC) were measured using a 3900 vibrating sample magnetometer (VSM). Different magnetic domain states of ferrimagnetic minerals, as well as varying interaction strengths, produce distinct distributions on FORC diagrams. The above experiments were performed in the Laboratory of Environmental Magnetism, Institute of Earth Environment, Chinese Academy of Sciences (Xi'an, China).

2.3 Geochemical analysis

Geochemical elements Rb, Sr, and Ti were analyzed at 5cm intervals using an Axios advanced wavelength dispersive X-ray fluorescence spectrometer (XRF). Titanium (Ti) is essentially insoluble and exhibits very limited mobility during weathering and transport. Therefore, it is commonly used as an indicator of terrigenous abundance in sediments. During chemical weathering, rubidium (Rb) is relatively immobile, whereas strontium (Sr) is readily leached. Consequently, the Rb/Sr ratio is widely used as an indicator of chemical weathering intensity (Jin et al., 2006; Perri, 2018). Reduced Rb/Sr ratios indicate increased chemical weathering, suggesting periods of stronger monsoon precipitation (Liu et al., 2023).

2.4 Spectral analysis

Xu et al. (2024) estimated the bottom age of the PT2 lacustrine sequence at ~184 ka; the sequence was time-calibrated using a paleomagnetic age-depth model. The series was then resampled to a uniform 1 ka grid and linearly detrended in Past 3.0 (Hammer and Harper, 2001). To extract Milankovitch and sub-Milankovitch signals, we applied Gaussian band-pass filters (Paillard et al., 1996). Frequency spectra information of the magnetic and geochemical proxies in core PT2 was obtained by

https://doi.org/10.5194/egusphere-2026-2154
Preprint. Discussion started: 23 April 2026

applying Welch's method to the evenly spaced data using the REDFIT spectrum program (Schulz and Mudelsee, 2002). The spectrum of Rb/Sr and ARM variations along the core was examined using continuous wavelet transforms in MATLAB (Torrence and Compo, 1998).

3 Results

3.1 Magnetic and geochemical proxies

The limited aeolian origin in Southwest China, together with surface soil studies (Hu et al., 2015), indicates that the primary sediment source of the Heqing Basin is fluvial transport within the catchment. The consistency of the magnetic proxies in our study further supports this interpretation (Fig. 2). The χ-T curves of all samples rapidly decrease around 580°C, and do not reach their minimum at 600°C (Fig. 3). Some samples from MIS 5 and MIS 6 also show a decline in the 300-400°C range (Fig. 3c, d). These observations suggest that the samples are primarily composed of magnetite and hematite, with some also containing maghemite (Deng et al., 2001; Shen et al., 2020). The FORC diagrams show low coercivity, suggesting that authigenic iron sulfides, such as greigite, are not formed (Chang et al., 2014; Qiang et al., 2018). The amplitudes and trends of magnetic and geochemical proxies vary across different MIS stages. Therefore, a correlation analysis was conducted (Fig. 4). ARM shows weaker correlations with some proxies. However, it remains correlated with χ ($R = 0.47$) and SIRM ($R = 0.71$) (Fig. 4), suggesting the SD grain signal plays a prominent role in ferrimagnetic minerals in core PT2. The FORC diagrams provide further evidence. Strongly magnetic samples display pronounced SD grain signals. In contrast, weakly magnetic samples show reduced SD signals together with enhanced SP signals (Liu et al., 2012). This highlights the significant contribution of SD grains to the lake sediments of core PT2. Moreover, the good correspondence between magnetic and geochemical proxies at peaks and troughs indicates that geochemical indicators also respond to ISM variability. The positive correlation between Ti and Rb/Sr values reflects a strong link between Rb/Sr ratios and terrigenous input, while also indicating an inverse relationship between physical and chemical weathering processes (Xu et al., 2010).

https://doi.org/10.5194/egusphere-2026-2154
Preprint. Discussion started: 23 April 2026

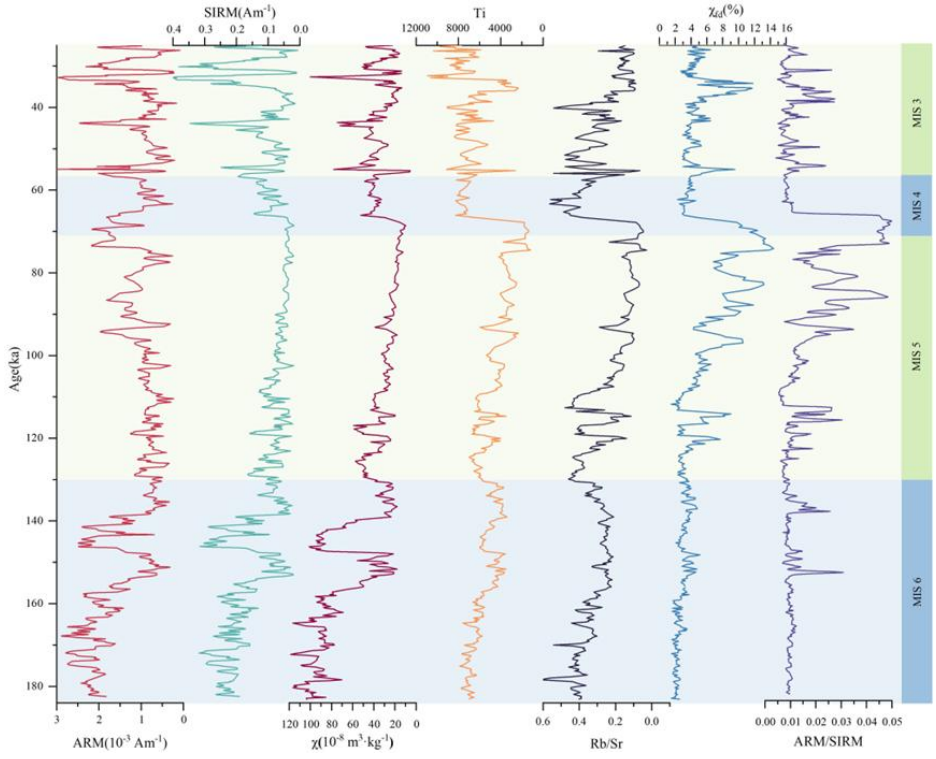

Figure 2: Magnetic and geochemical records from the PT2 drill core.

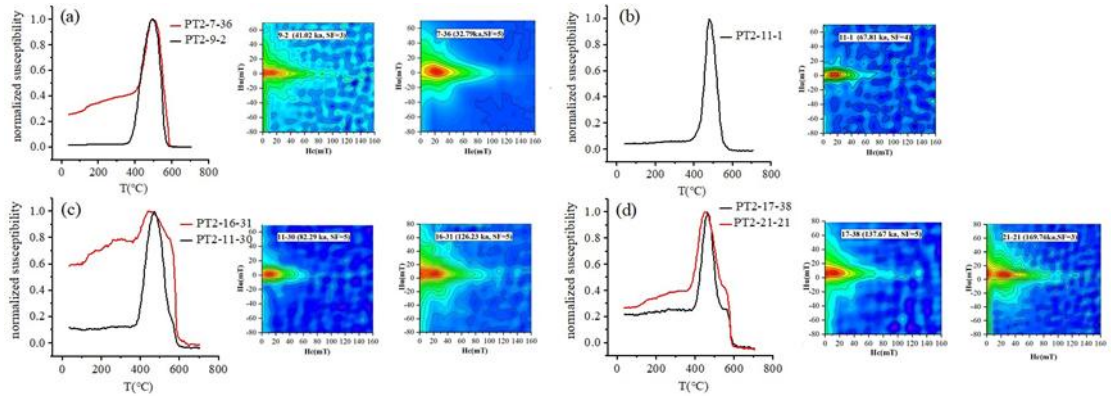

Figure 3: χ-T curves and FORC diagrams of representative samples from the PT2 lacustrine core during MIS 3-6: (a) magnetically weak and strong samples from MIS3; (b) magnetically weak samples from MIS4; (c) magnetically weak and strong samples from MIS5; (d) magnetically weak and strong samples from MIS6.

https://doi.org/10.5194/egusphere-2026-2154
Preprint. Discussion started: 23 April 2026

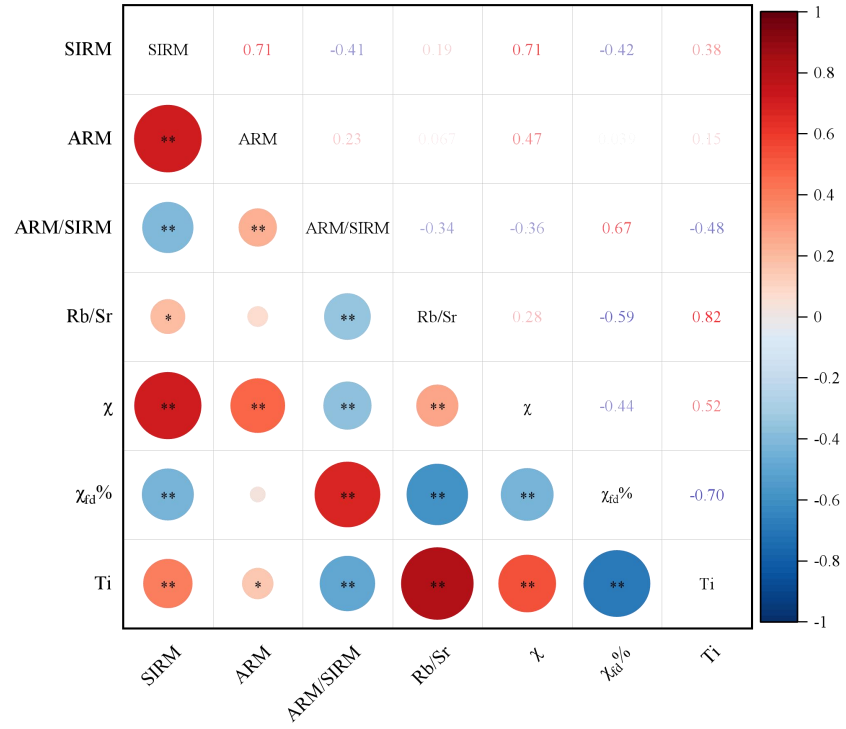

Figure 4: Statistical correlation between magnetic and geochemical proxies in PT2.

p≤0.05(*), p≤0.01(**)

3.2 Spectral analysis

Spectral and wavelet analyses show that ARM in the PT2 core is dominated by a significant ~20 ka cycle (Fig. 5, 6). The band-pass filtering results further demonstrate a close correspondence between ARM and precession (Fig. 7). This dominant precessional signal is consistent with speleothem $\delta^{18}O$ records from Xiaobailong Cave (XBL, 24°12′N, 103°21′E) (Cheng et al., 2016), Bittoo Cave (30°47′N, 77°46′E) (Kathayat et al., 2016), and Sanbao Caves (SBD, 31°40′N, 110°26′E) (Wang et al., 2008) (Fig. 8). Among the magnetic proxies, ARM shows the strongest precession-scale signal, whereas ARM/SIRM and χfd% display more pronounced glacial–interglacial variability. χ and SIRM preserve both precession and glacial–interglacial variability (Fig. 5). Spectral and wavelet analyses of Rb/Sr likewise identify a significant ~100 ka periodicity (Figs. 5, 6), and the band-pass filtering results show that Rb/Sr closely tracks glacial–interglacial variability (Fig. 7). More broadly, the PT2 proxy records correspond well with the Greenland Ice-Core Project (GRIP) $\delta^{18}O$ record (Dansgaard et al., 1993), the Antarctic Temperature Stack (ATS) (Frédéric Parrenin et al., 2013), and the Indian Ocean sea-surface temperature record from core MD90963 (Bassinot et al., 1994), all of which are characterized by pronounced glacial–interglacial variability over 184–25 ka (Fig. 8).

https://doi.org/10.5194/egusphere-2026-2154
Preprint. Discussion started: 23 April 2026

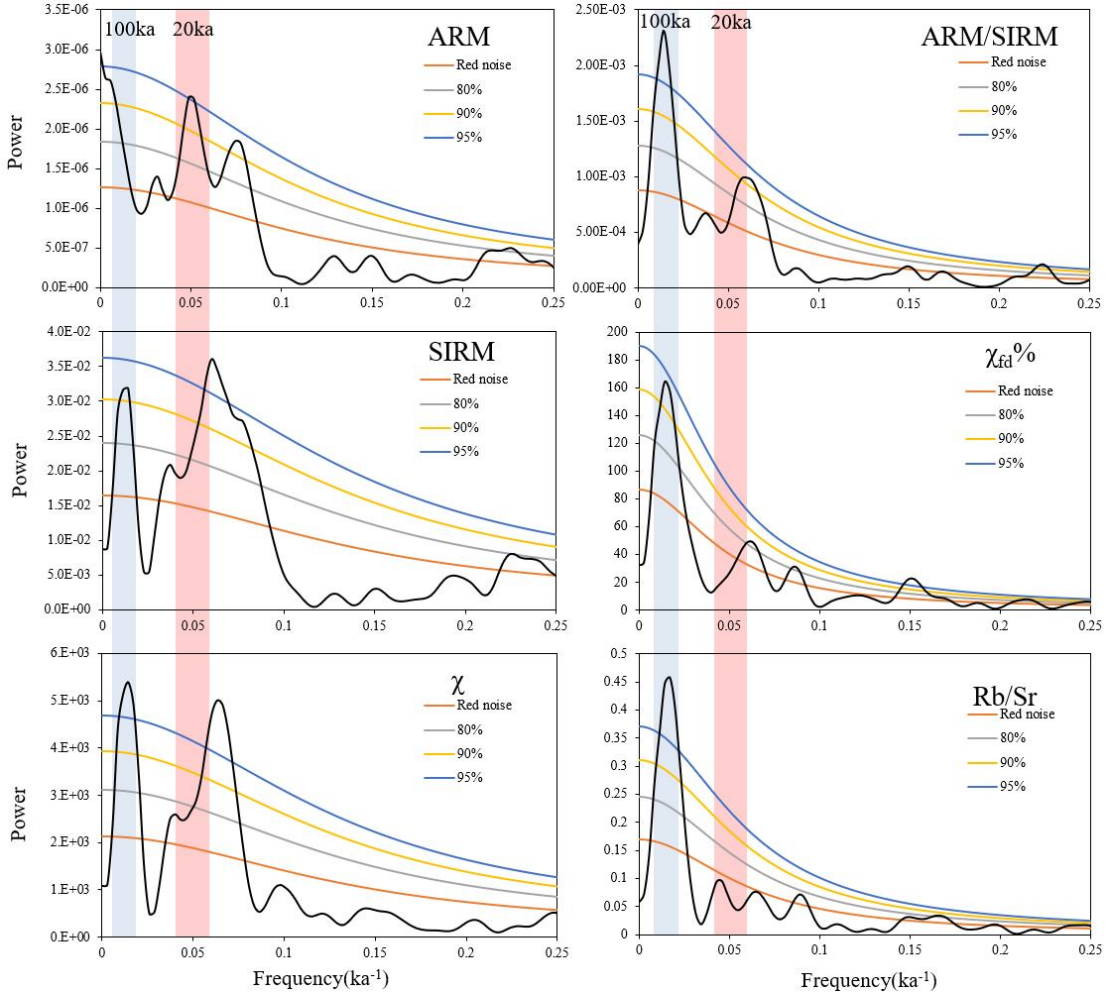

Figure 5: Spectral analysis results performed on ARM, SIRM, χ, ARM/SIRM, χfd%, and Rb/Sr data from core PT2. Orange, gray, yellow, and blue lines represent theoretical red noise, 80%, 90%, and 95% false-alarm levels, respectively. The analysis was performed using the REDFIT spectral analysis program. The age range of the precession cycle (~20 ka) and glacial-interglacial cycle (~100 ka) has also been marked.

https://doi.org/10.5194/egusphere-2026-2154
Preprint. Discussion started: 23 April 2026

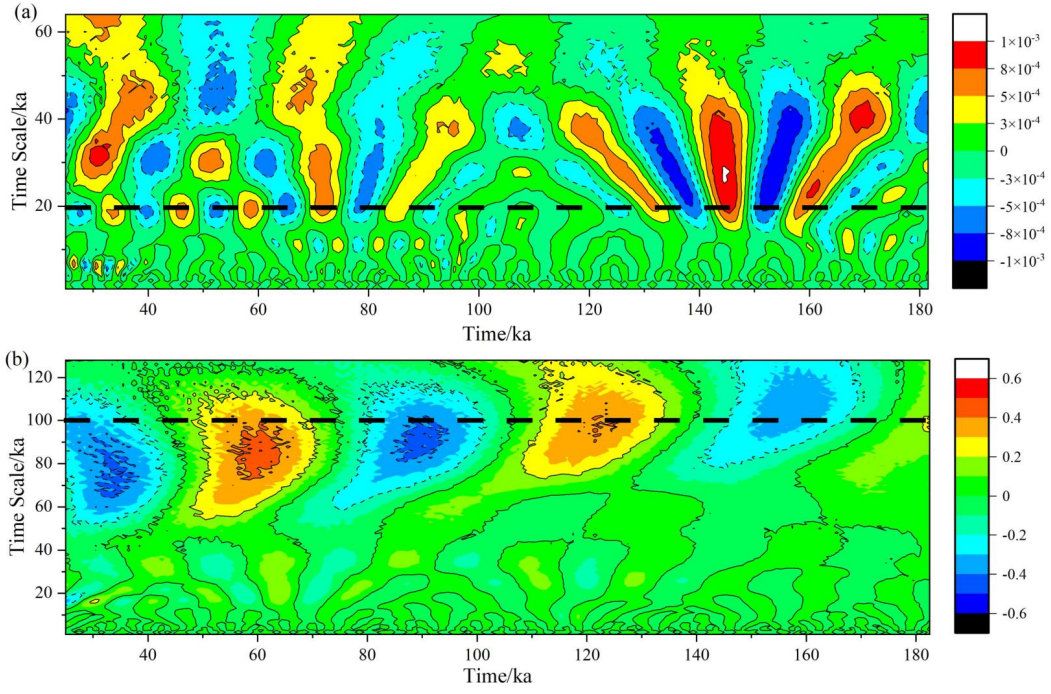

Figure 6: Comparison of continuous wavelet analysis results of ARM and Rb/Sr records during 184-25 ka B.P. Cool-to-warm colors indicate low-to-high wavelet modulus strength at different scales. Black dashed lines mark the precession cycles (~20 ka) and the glacial-interglacial cycles (~100 ka).

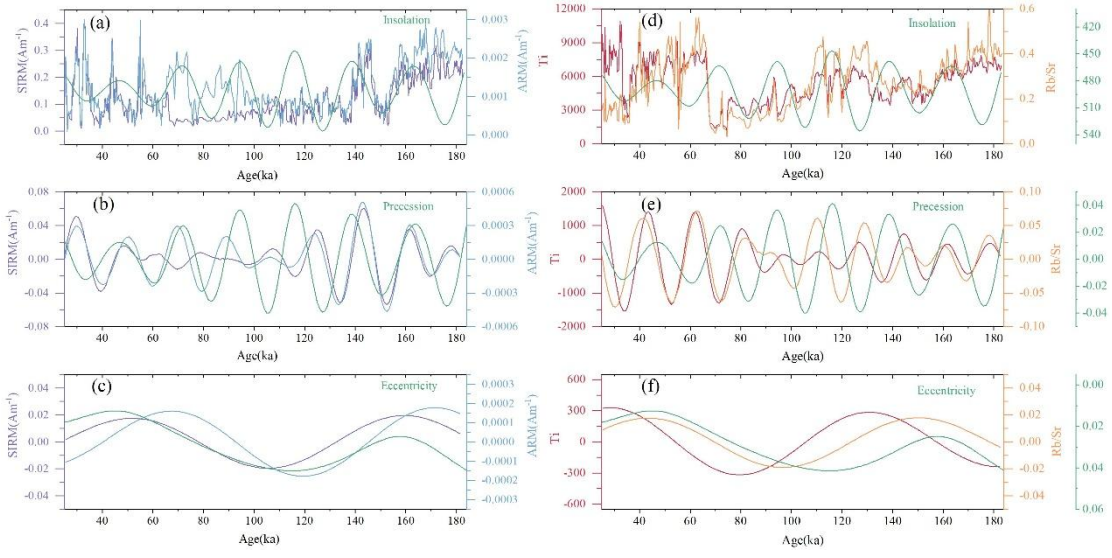

Figure 7: Time series of magnetic and geochemical records of core PT2. (a) Time series of the SIRM (purple, left scale) and ARM (blue, right scale) records of core PT2. (b) Precession cycle filter for the SIRM (purple, left scale) and ARM (blue, right scale) records of core PT2. (c) is the same as (b) but for the glacial-interglacial cycles filter. (d) Time series of the Ti (red, left scale) and Rb/Sr (orange, right scale) records of core PT2. (e) Precession cycle filter for Ti and Rb/Sr records of core PT2. (f) is the same as (e) but for the glacial-interglacial cycles filter. The green line in (a), (d) is for NHSI at 30°N, in (b), (e) is for the precession parameter, while in (c), (f) is for the glacial-interglacial cycles.

https://doi.org/10.5194/egusphere-2026-2154
Preprint. Discussion started: 23 April 2026

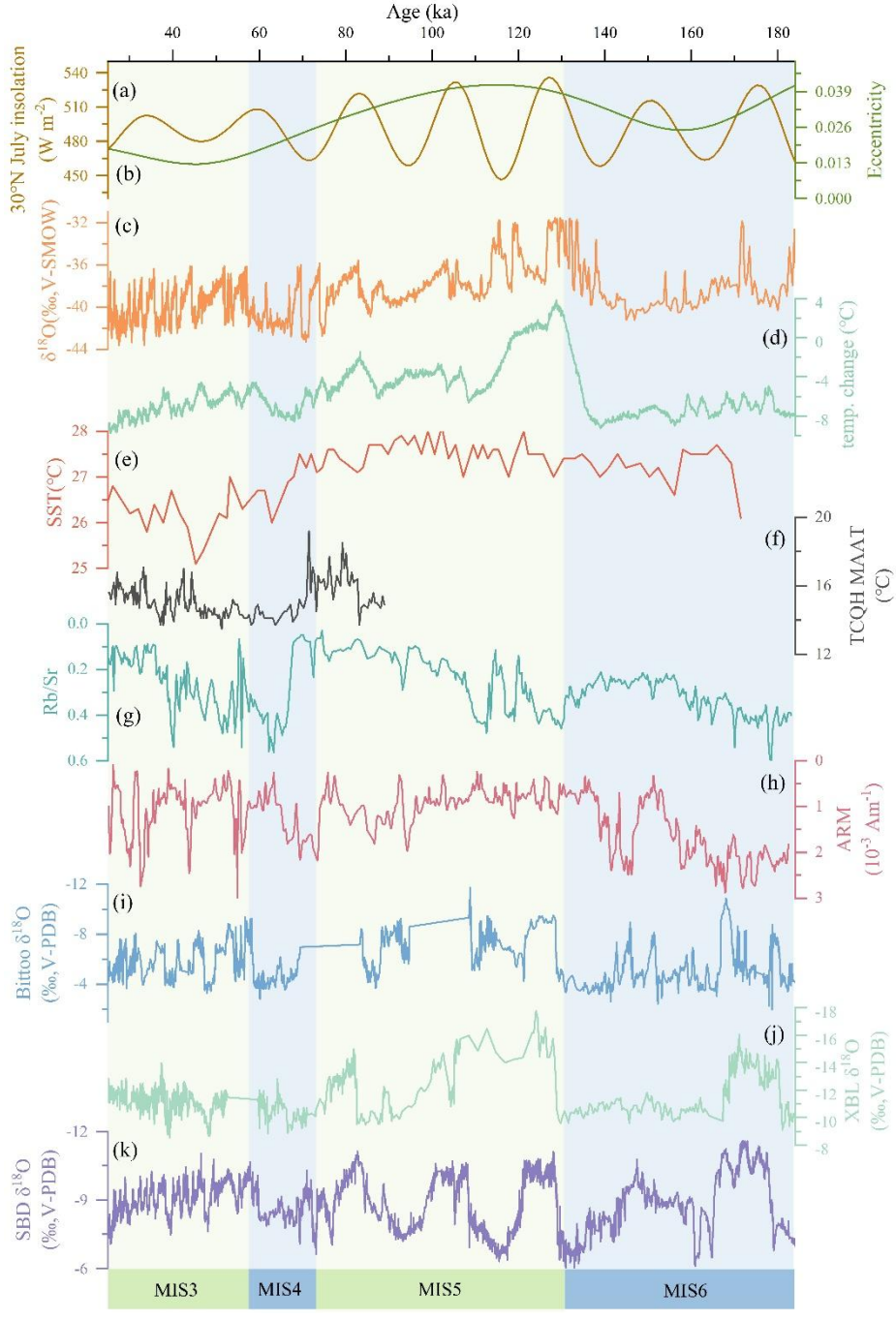

Figure 8: Comparisons among the magnetic and geochemical records of core PT2 and other global climatic records during 184-25 ka. (a) 30°N Summer Insolation; (b) eccentricity cycle; (c) $\delta^{18}O$ records in Greenland Ice-Core Project (GRIP) ice core(Dansgaard et al., 1993); (d) Antarctic Temperature Stack (ATS) records(F. Parrenin et al., 2013); (e) SST variations in the Indian Ocean(Bassinot et al., 1994); (f) Lake Tengchongqinghai (TCQH) MAAT record(Zhao et al., 2021); (g) and (h) Rb/Sr and ARM records of core PT2; (i) Bittoo $\delta^{18}O$ records(Kathayat et al., 2016); (j) XBL $\delta^{18}O$ record(Cheng et al., 2016); (k) SBD $\delta^{18}O$ records(Wang et al., 2008).

https://doi.org/10.5194/egusphere-2026-2154
Preprint. Discussion started: 23 April 2026

4 Discussion

In southwestern China, moisture is delivered mainly by the ISM, which transports water vapor from the Indian Ocean, including the Arabian Sea and the Bay of Bengal (Cai et al., 2015; Zhang, 2020). The Heqing Basin lies on the southeastern margin of the Tibetan Plateau, within a climatically sensitive transition zone where the ISM interacts with the East Asian summer monsoon (EASM) (Hu et al., 2015; Xu et al., 2020). Previous studies suggest that the magnetic minerals in Heqing lacustrine sediments are derived mainly from catchment detrital input (Hu et al., 2015; Xu et al., 2024). Under stronger ISM conditions in the Heqing Basin, denser catchment vegetation tends to reduce physical erosion and the delivery of coarse detrital material to the lake, while wetter conditions enhance chemical weathering (Mishra et al., 2019; Wang et al., 2020). These changes lead to lower detrital input and lower concentrations of magnetic minerals, reflected by reduced Ti, χ, ARM, and SIRM values. At the same time, the magnetic grain-size distribution shifts toward finer fractions, increasing the relative abundance of fine SD/SP particles, as indicated by higher ARM/SIRM and χfd% values (Su et al., 2019; Tan et al., 2020). Conversely, weaker ISM intervals are characterized by stronger physical erosion, greater input of coarser detrital material, higher concentration-dependent parameters, and lower fine-grain-sensitive ratios. These magnetic parameters do not record precipitation directly, but can serve as indirect proxies for ISM-related hydroclimatic variability by tracking changes in catchment weathering, erosion, and the flux and grain size of detrital material delivered to the lake (Hu et al., 2015; Wang et al., 2021). However, individual magnetic parameters differ in sensitivity and reliability, so it is necessary to identify the most suitable proxy for the PT2 core.

ARM has been widely applied in lake sediment paleoclimate studies as an indicator of the content of fine ferrimagnetic grains, owing to its sensitivity to SD particles (Liu et al., 2012). Ratios such as ARM/SIRM and ARM/χ are commonly used to assess variations in the concentration of fine-grained magnetic particles. In environmental magnetic studies of loess, alluvial, and lacustrine sediments, ARM and its derived ratios often show significant correlations with annual precipitation and soil moisture (Hu et al., 2015; Nie et al., 2016; Zan et al., 2018). Therefore， it was employed as monsoon intensity and precipitation proxy (Basavaiah et al., 2014; King et al., 1983). By contrast, χ can be affected by post-depositional alteration, including the dissolution of fine magnetic minerals, which may weaken the environmental signal it records (Liu et al., 2012; Snowball, 1993). Moreover, where χ exhibits only limited variability, its usefulness for quantitative and spectral analyses is reduced (Schulz and Mudelsee, 2002; Weedon, 2022). In the PT2 core, rock magnetic results indicate a substantial contribution from SD particles, and ARM covaries closely with χ and SIRM. These observations suggest that ARM reliably tracks changes in magnetic mineral input and grain size. In addition, the close correspondence between ARM and the $\delta^{18}O$ records from XBL, SBD, and Bittoo caves indicates that ARM captures hydroclimatic variability closely linked to ISM change. During precession-index minima, when perihelion coincides with boreal summer, Northern Hemisphere summer insolation increases, strengthening monsoon circulation and shifting the ITCZ northward (Cai et al., 2015; Cheng et al., 2021; Dong et al., 2025; Tabor et al., 2018). This enhances moisture transport to southwestern China and increases regional precipitation (Wen et al., 2022; Zhang et al., 2023). In the PT2 core, these wetter conditions are associated with lower

https://doi.org/10.5194/egusphere-2026-2154
Preprint. Discussion started: 23 April 2026

magnetic mineral concentrations and reduced ARM values (Fig. 8). These results suggest that ARM may be the most suitable magnetic proxy for reconstructing monsoon- and precipitation-related environmental changes in the PT2 core.

However, the paleoclimate indicators in the PT2 core respond differently to orbital forcing: ARM is dominated by a precession-scale (~20 ka) cycle, whereas Rb/Sr shows stronger glacial–interglacial (~100 ka) variability (Fig. 5, 6). This contrast likely reflects differences in their environmental significance, sensitivity, and recording mechanisms. Previous studies have shown that fine-grained magnetic proxies, especially ARM and related ratios, can display clear precessional variability in ISM records (Chen et al., 2022; Xu et al., 2025). ARM is particularly sensitive to SD particles and therefore responds readily to changes in the abundance and grain size of fine magnetic particles (Egli and Lowrie, 2002; Liu et al., 2012). In ISM settings, runoff, erosion, and sediment transport strongly influence the flux and grain-size distribution of catchment-derived fine detritus delivered to lakes. ARM can therefore more readily capture precession-paced hydroclimatic variability through changes in the input of fine magnetic particles (Xu et al., 2025; Zhong et al., 2018). Rb/Sr, in contrast, reflects more integrated catchment processes, including chemical weathering intensity, sediment source composition, and catchment denudation (Liu et al., 2023; Xu et al., 2010). Because these processes evolve over longer timescales and involve substantial storage and mixing within the catchment, Rb/Sr tends to emphasize low-frequency glacial–interglacial variability. Precession-scale variability may still be present in the Rb/Sr record, but it is likely much weaker than the dominant low-frequency signal. Moreover, the close correspondence of Rb/Sr with the Lake Tengchongqinghai (TCQH) MAAT record (Zhao et al., 2021), the Antarctic Temperature Stack (ATS) records (F. Parrenin et al., 2013), and Indian Ocean SST records (Bassinot et al., 1994) suggests that Rb/Sr was more sensitive to the slowly varying glacial–interglacial background state than to precession-paced monsoon forcing(An et al., 2011; Jin et al., 2006). As glacial–interglacial conditions changed, moisture availability, vegetation cover, weathering intensity, and erosion regime also shifted systematically. These changes likely enhanced the glacial–interglacial variability of Rb/Sr. During glacial periods, expanded ice sheets and lower sea level weakened the ISM and reduced moisture delivery to southwest China, resulting in colder and drier catchment conditions. Under these conditions, chemical weathering was suppressed, whereas physical erosion and terrigenous detrital input became relatively more important, leading to elevated Rb/Sr ratios (Liu et al., 2023; Xu et al., 2010). During interglacial periods, by contrast, a stronger ISM would have increased regional effective moisture and promoted warmer and more humid conditions in the basin. These conditions favored more intense chemical weathering and enhanced Sr mobilization from source materials, leading to lower Rb/Sr ratios (An et al., 2011; Clemens et al., 2021).

Such proxy-dependent differences are also observed within the magnetic record (Fig. 5). During MIS 5, when χ and SIRM show relatively limited variability, whereas ARM exhibits more pronounced changes (Fig. 2). Ti values are markedly low during this interval (Fig. 2), and the FORC diagrams show pronounced SD characteristics (Fig. 3c), indicating persistently low detrital input and a relative enrichment of fine magnetic grains. In this setting, ARM becomes more closely associated with fine-grained magnetic indicators such as χfd% and ARM/SIRM, rather than with χ and SIRM as in most other intervals. This difference likely reflects the contrasting sensitivities of these proxies: χ and SIRM mainly track bulk magnetic mineral concentration, whereas ARM is more sensitive to stable single-domain (SSD) grains and small vortex-state particles (Liu et

https://doi.org/10.5194/egusphere-2026-2154
Preprint. Discussion started: 23 April 2026

al., 2012). As a result, ARM during MIS 5 was likely influenced more by magnetic grain-size variations than by concentration alone, which may explain why it preserves a stronger precession-scale signal than the other magnetic proxies (Kanu et al., 2019; Liu et al., 2012; Zhang et al., 2025).

In addition to climatic forcing, post-depositional processes may also have contributed to the orbital-scale differences between ARM and Rb/Sr. Alternatively, reductive dissolution is likely to have been particularly important, given its widespread occurrence in lacustrine sediments of the Heqing Basin (Hu et al., 2015; Snowball, 1993; Zan et al., 2018; Zhang et al., 2012). Under anoxic conditions, maghemite is more susceptible to dissolution than magnetite (Wang et al., 2021; Williamson et al., 1998; Xu et al., 2020; Zan et al., 2018). In the PT2 core, samples from MIS 5 and MIS 6 show a decrease in χ between 300 and 400°C on the χ-T curves, consistent with the presence of maghemite (Deng et al., 2000), whereas this feature is absent in samples from MIS 3 and MIS 4. This pattern suggests that maghemite was better preserved during MIS 5–6, but more extensively dissolved during MIS 3–4. Reductive dissolution likely modulated the amplitude and variability of some magnetic parameters, especially those sensitive to fine ferrimagnetic grains, such as ARM/SIRM and χfd%, but did not fundamentally erase their orbital-scale signal. The broad agreement among magnetic proxies, and their overall consistency with geochemical records, indicates that the main climatic signal remains preserved. Magnetic proxies such as ARM therefore remain useful for reconstructing monsoon-related environmental change, although interpretations are more robust when supported by multiproxy comparisons.

5 Conclusions

In the PT2 core from the Heqing Basin, magnetic and geochemical proxies record coherent environmental changes from 25 to 184 ka. Rock-magnetic results suggest that SD and small vortex-state particles are the dominant magnetic domain states in the sediments. The close covariation of ARM with χ and SIRM further supports the use of ARM as the most suitable magnetic proxy for reconstructing environmental change. Among the measured proxies, ARM exhibits the clearest precession-scale variability (~20 ka), consistent with the $\delta^{18}O$ records from XBL, Bittoo, and SBD Cave. By contrast, Rb/Sr is dominated by glacial–interglacial variability and shows closer agreement with the TCQH MAAT, ATS, and Indian Ocean SST records. These contrasting orbital periodicities likely reflect differences in proxy sensitivity and recording mechanisms. ARM mainly responds to relatively rapid hydroclimatic processes associated with precipitation-driven erosion and fine-particle transport, whereas Rb/Sr more strongly reflects slower changes in weathering and catchment response. The contrast among magnetic proxies is especially evident during MIS 5. During this interval, low detrital input and a relative enrichment of fine magnetic grains likely caused ARM to be influenced more by magnetic grain-size variations than by concentration alone, allowing a clearer precession-scale signal to be preserved. Although reductive dissolution likely modified the amplitude of some magnetic parameters, it did not fundamentally overprint the primary orbital-scale structure of the record. These results highlight the value of ARM as a robust proxy for precession-paced monsoon variability in the Heqing Basin and emphasize the importance of multiproxy comparisons for interpreting orbital-scale environmental change.

https://doi.org/10.5194/egusphere-2026-2154
Preprint. Discussion started: 23 April 2026

Code and data availability

The data in this paper can be obtained by contacting the corresponding author (xuxinwen@nwu.edu.cn).

Author contributions

ZY, XX and XQ developed the research idea. ZY prepared the manuscript with contributions from XX and all the other co-authors. SL and JZ led the formal analysis. ZY and LL contributed with figures preparation. All authors contributed to article development and revision.

Competing interests

The contact author has declared that none of the authors has any competing interests.

Disclaimer

Publisher's note: Copernicus Publications remains neutral with regard to jurisdictional claims made in the text, published maps, institutional affiliations, or any other geographical representation in this paper. The authors bear the ultimate responsibility for providing appropriate place names. Views expressed in the text are those of the authors and do not necessarily reflect the views of the publisher.

Acknowledgements

The authors are grateful to all those who have enabled this work by collecting, measuring, collating, and screening magnetic and geochemical data.

Financial support

This research was funded jointly by the National Natural Science Foundation of China (42172203, 41402151), and the Open Fund of the State Key Laboratory of Loess and Quaternary Geology (SKLLQG2009).

https://doi.org/10.5194/egusphere-2026-2154
Preprint. Discussion started: 23 April 2026

References

An, Z.S., Clemens, S.C., Shen, J., Qiang, X.K., Jin, Z.D., Sun, Y.B., Prell, W.L., Luo, J.J., Wang, S.M., Xu, H., Cai, Y.J., Zhou, W.J., Liu, X.D., Liu, W.G., Shi, Z.G., Yan, L.B., Xiao, X.Y., Chang, H., Wu, F., Ai, L., Lu, F.Y., 2011. Glacial-Interglacial Indian Summer Monsoon Dynamics. Science. https://doi.org/10.1126/science.1203752.

Bajo, P., Drysdale, R.N., Woodhead, J.D., Hellstrom, J.C., Hodell, D., Ferretti, P., Voelker, A.H.L., Zanchetta, G., Rodrigues, T., Wolff, E., Tyler, J., Frisia, S., Spötl, C., Fallick, A.E. 2020. Persistent influence of obliquity on ice age terminations since the Middle Pleistocene transition. Science, 367(6483), 1235-1239. https://doi.org/doi:10.1126/science.aaw1114.

Basavaiah, N., Wiesner, M.G., Anoop, A., Menzel, P., Nowaczyk, N.R., Deenadayalan, K., Brauer, A., Gaye, B., Naumann, R., Riedel, N., Stebich, M., Prasad, S., 2014. Physicochemical analyses of surface sediments from the Lonar Lake, central India-implications for palaeoenvironmental reconstruction. Fundamental and Applied Limnology / Archiv für Hydrobiologie, 184, 51-68. https://doi.org/10.1127/1863-9135/2014/0515.

Bassinot, F.C., Labeyrie, L.D., Vincent, E., Quidelleur, X., Shackleton, N.J., Lancelot, Y., 1994. The astronomical theory of climate and the age of the Brunhes-Matuyama magnetic reversal. Earth and Planetary Science Letters. https://doi.org/10.1016/0012-821x(94)90244-5.

Berger, A., 1978. Long-term variations of daily insolation and Quaternary climatic changes. Journal of Atmospheric Sciences, 35(12), 2362-2367. https://doi.org/10.1175/1520-0469(1978)035%3C2362:LTVODI%3E2.0.CO;2.

Cai, Y.J., Fung, I.Y., Edwards, R.L., An, Z.S., Cheng, H., Lee, J.E., Tan, L.C., Shen, C.C., Wang, X.F., Day, J.A., Zhou, W.J., Kelly, M.J., Chiang, J.C.H., 2015. Variability of stalagmite-inferred Indian monsoon precipitation over the past 252,000 y. Proceedings of the National Academy of Sciences of the United States of America. https://doi.org/10.1073/pnas.1424035112.

Chang, L., Vasiliev, I., van Baak, C., Krijgsman, W., Dekkers, M.J., Roberts, A.P., Gerald, J.D.F., van Hoesel, A., Winklhofer, M., 2014. Identification and environmental interpretation of diagenetic and biogenic greigite in sediments: A lesson from the Messinian Black Sea. Geochemistry Geophysics Geosystems, 15(9), 3612-3627. https://doi.org/10.1002/2014gc005411.

Chen, L., Guan, Y., Zhou, L., Yin, Z., & Jiang, Z., 2022. Variability of Indian monsoon and its forcing mechanisms since late quaternary. Frontiers in Earth Science, 10, 977250. https://10.3389/feart.2022.977250.

Cheng, H., Edwards, R.L., Sinha, A., Spötl, C., Yi, L., Chen, S., Kelly, M., Kathayat, G., Wang, X.F., Li, X.L., Kong, X.G., Wang, Y.J., Ning, Y.F., Zhang, H.W., 2016. The Asian monsoon over the past 640,000 years and ice age terminations. Nature. https://doi.org/10.1038/nature18591.

Cheng, H., Zhang, H.W., Cai, Y.J., Shi, Z.G., Yi, L., Deng, C.L., Hao, Q.Z., Peng, Y.B., Sinha, A., Li, H.Y., Zhao, J.Y., Tian, Y., Baker, J., Perez-Mejías, C., 2021. Orbital-scale Asian summer monsoon variations: Paradox and exploration. Science China Earth Sciences, 64(4), 529-544. https://doi.org/10.1007/s11430-020-9720-y.

https://doi.org/10.5194/egusphere-2026-2154
Preprint. Discussion started: 23 April 2026

Clemens, S.C., Yamamoto, M., Thirumalai, K., Giosan, L., Richey, J.N., Nilsson-Kerr, K., Rosenthal, Y., Anand, P., McGrath, S.M., 2021. Remote and local drivers of Pleistocene South Asian summer monsoon precipitation: A test for future predictions. Science Advances. https://doi.org/10.1126/sciadv.abg3848.

Dansgaard, W., Johnsen, S.J., Clausen, H.B., Dahl-Jensen, D., Gundestrup, N.S., Hammer, C.U., Hvidberg, C.S., Steffensen, J.P., Sveinbjörnsdottir, A.E., Jouzel, J., Bond, G., 1993. Evidence for general instability of past climate from a 250-kyr ice-core record. Nature. https://doi.org/10.1038/364218a0.

Deng, C.L, Zhu, R.X, Jackson, M.J., Verosub, K.L., Singer, M.J., 2001. Variability of the temperature-dependent susceptibility of the Holocene eolian deposits in the Chinese loess plateau: A pedogenesis indicator . Physics and Chemistry of the Earth Part a-Solid Earth and Geodesy, 26(11-12), 873-878. https://doi.org/10.1016/s1464-1895(01)00135-1.

Deng, C.L., Zhu, R.X., Verosub, K.L., Singer, M.J., Yuan, B.Y., 2000. Paleoclimatic significance of the temperature-dependent susceptibility of Holocene loess along a NW-SE transect in the Chinese loess plateau. Geophysical Research Letters 27, 3715–3718. https://doi.org/10.1029/2000GL008462

Dong, X.Y., Zhang, X., Zhang, H.W., Zhang, Y.A., Rasmussen, S.O., Zhang, R., Cai, Y.J., Huang, S.Y., Kathayat, G., Pérez-Mejías, C., Zong, B.Y., Liu, D.B., Duan, P.Z., Svensson, A., Spötl, C., Li, Y.W., Niu, X.W., Wang, J., Li, H.Y., Ning, Y.F., Xu, Y., Wang, X.F., Stríkis, N.M., Cruz, F.W., Sinha, A., Werner, M., Lawrence Edwards, R., Cheng, H., 2025. Interstadial diversity of East Asian summer monsoon linked to changes of the Northern Westerlies. Nature Communications, 16(1), 7765. https://doi.org/10.1038/s41467-025-63057-2.

Egli R, Lowrie W., 2002. Anhysteretic remanent magnetization of fine magnetic particles. Journal of Geophysical Research: Solid Earth, 107(B10): EPM 2-1-EPM 2-21. https://doi.org/10.1029/2001JB000671.

Guo, Y.L., Yang, S.Y., Su, N., Li, C., Yin, P., Wang, Z.B., 2018. Revisiting the effects of hydrodynamic sorting and sedimentary recycling on chemical weathering indices. Geochimica et Cosmochimica Acta, 227, 48-63. https://doi.org/10.1016/j.gca.2018.02.015.

Hicks, S., 2006. When no pollen does not mean no trees. Vegetation History and Archaeobotany, 15(4), 253-261. https://doi.org/10.1007/s00334-006-0063-9.

Hu, S.Y., Goddu, S.R., Herb, C., Appel, E., Gleixner, G., Wang, S.M., Yang, X.D., Zhu, X.H., 2015. Climate variability and its magnetic response recorded in a lacustrine sequence in Heqing basin at the SE Tibetan Plateau since 900 ka. Geophysical Journal International. https://doi.org/10.1093/gji/ggv033.

Huang, Y.S., Lee, T.Q., Hsu, S.K., 2015. Orbital-scale variation in the magnetic content as a result of sea level changes in Papua New Guinea over the past 400 ka. Earth, Planets and Space, 67(1), 128. https://doi.org/10.1186/s40623-015-0300-5.

Jin, Z.D., Cao, J.J., Wu, J.L., Wang, S.M., 2006. A Rb/Sr record of catchment weathering response to Holocene climate change in Inner Mongolia. Earth Surface Processes and Landforms: The Journal of the British Geomorphological Research Group, 31(3), 285-291. https://doi,org/10.1002/esp.1243.

Kanu, M.O., Meludu, O., Basavaiah, N., Oniku, A., 2019. Relationship between mineral magnetic properties and soil textural parameters. Acta Geophysica, 67(2), 517-532. https://doi,org/10.1007/s11600-019-00248-8.

https://doi.org/10.5194/egusphere-2026-2154
Preprint. Discussion started: 23 April 2026

Kathayat, G., Cheng, H., Sinha, A., Spötl, C., Edwards, R.L., Zhang, H.W., Li, X.L., Yi, L., Ning, Y.F., Cai, Y.J., Lui, W.L., Breitenbach, S.F.M., 2016. Indian monsoon variability on millennial-orbital timescales. Scientific Reports. https://doi.org/10.1038/srep24374.

King, J.W., Banerjee, S.K., Marvin, J., 1983. A new rock - magnetic approach to selecting sediments for geomagnetic paleointensity studies: Application to paleointensity for the last 4000 years. Journal of Geophysical Research: Solid Earth, 88(B7), 5911-5921. https://doi.org/10.1029/jb088ib07p05911.

Laskar, J., Robutel, P., Joutel, F., Gastineau, M., Correia, A.C.M., Levrard, B. 2004. A long-term numerical solution for the insolation quantities of the Earth. Astronomy & Astrophysics. https://doi.org/10.1051/0004-6361:20041335.

Li, C., Yang, S.Y., 2010. Is chemical index of alteration (CIA) a reliable proxy for chemical weathering in global drainage basins? American Journal of Science, 310(2), 111-127. https://doi.org/10.2475/02.2010.03.

Li, D., Tan, L.C, Cai, Y.J., Jiang, X.Y., Ma, L., Cheng, H., Edwards, R.L., Zhang, H.W., Gao, Y.L., An, Z.S., 2019. Is Chinese stalagmite δ18O solely controlled by the Indian summer monsoon? Climate Dynamics, 53(5), 2969-2983. https://doi.org/10.1007/s00382-019-04671-x.

Li, J.Y., Zhao, Y., Xu, Q.H., Zheng, Z., Lu, H.Y., Luo, Y.L., Li, Y.C., Li, C.H., Seppä, H., 2014. Human influence as a potential source of bias in pollen-based quantitative climate reconstructions. Quaternary Science Reviews, 99, 112-121. https://doi.org/https://doi.org/10.1016/j.quascirev.2014.06.005.

Li, T., Liu, F., Abels, H.A., You, C.F., Zhang, Z., Chen, J., Ji, J.F., Li, L.F., Li, L., Liu, H.C., 2017. Continued obliquity pacing of East Asian summer precipitation after the mid-Pleistocene transition. Earth and Planetary Science Letters, 457, 181-190. https://doi.org/10.1016/j.epsl.2016.09.045.

Li, X.S., Zhou, Y.W., Han, Z.Y., Yuan, X.K., Yi, S.W., Zeng, Y.Q., Qin, L.S., Lu, M., Lu, H.Y., 2024. Loess deposits in the low latitudes of East Asia reveal the~ 20-kyr precipitation cycle. Nature Communications, 15(1), 1023. https://doi.org/10.1038/s41467-024-45379-9.

Lisiecki, L.E., Raymo, M.E., 2005. A Pliocene - Pleistocene stack of 57 globally distributed benthic δ18O records. Paleoceanography, 20(1). https://doi.org/10.1029/2004pa001071.

Liu, L.P., Yu, K.K., Li, A.Z., Zhang, C., Wang, L., Liu, X.X., Lan, J.H., 2023. Weathering intensity response to climate change on decadal scales: A record of Rb/Sr ratios from Chaonaqiu Lake sediments, western Chinese Loess Plateau. Water, 15(10), 1890. https://doi.org/10.3390/w15101890.

Liu, Q.S., Roberts, A.P., Larrasoaña, J.C., Banerjee, S.K., Guyodo, Y., Tauxe, L., Oldfield, F., 2012. Environmental Magnetism: Principles and Applications. Reviews of Geophysics. https://doi.org/10.1029/2012RG000393.

Milankovitch, M., 1941. Canon of insolation and the iceage problem. Koniglich Serbische Akademice Beograd Special Publication, 132.

Mishra A K, Placzek C, Jones R., 2019. Coupled influence of precipitation and vegetation on millennial-scale erosion rates derived from 10Be. PloS one, 14(1): e0211325. https://doi.org/10.1371/journal.pone.0211325.

https://doi.org/10.5194/egusphere-2026-2154
Preprint. Discussion started: 23 April 2026

Nie J, Song Y and King JW., 2016. A Review of Recent Advances in Red-Clay Environmental Magnetism and Paleoclimate History on the Chinese Loess Plateau. Front. Earth Sci. 4:27. https://doi.org/10.3389/feart.2016.00027.

Paillard, D., Labeyrie, L., Yiou, P., 1996. Macintosh program performs time - series analysis. Eos, Transactions American Geophysical Union, 77(39), 379-379. https://doi.org/10.1029/96EO00259.

Parrenin, F., Masson-Delmotte, V., Köhler, P., Raynaud, D., Paillard, D., Schwander, J., Barbante, C., Landais, A., Wegner, A., Jouzel, J., 2013. Synchronous change of atmospheric CO2 and Antarctic temperature during the last deglacial warming. Science 339, 1060–1063. https://doi.org/10.1126/science.1226368.

Perri, F., 2018. Reconstructing chemical weathering during the Lower Mesozoic in the Western-Central Mediterranean area: a review of geochemical proxies. Geological Magazine, 155(4), 944-954. https://doi.org/10.1017/s0016756816001205.

Qiang, X.K., Xu, X.W., Zhao, H., Fu, C.F., 2018. Greigite formed in early Pleistocene lacustrine sediments from the Heqing Basin, southwest China, and its paleoenvironmental implications. Journal of Asian Earth Sciences, 156, 256-264. https://doi.org/10.1016/j.jseaes.2018.01.033.

Roberts, A.P., 2015. Magnetic mineral diagenesis. Earth-Science Reviews, 151, 1-47. https://doi.org/10.1016/j.earscirev.2015.09.010.

Saadeh, C.M., Saylor, J.E., Nie, J., Shanahan, T.M., 2020. Orbital forcing of late Miocene-early Pleistocene environmental change in the Zhada Basin, SW Tibetan Plateau. Paleoceanography and Paleoclimatology, 35(8), e2019PA003781. https://doi.org/10.1029/2019PA003781.

Sandeep, K., Shankar, R., Warrier, A.K., Yadava, M.G., Ramesh, R., Jani, R.A., Weijian, Z., Xuefeng, L., 2017. A multi-proxy lake sediment record of Indian summer monsoon variability during the Holocene in southern India. Palaeogeography, Palaeoclimatology, Palaeoecology, 476, 1-14. https://doi.org/10.1016/j.palaeo.2017.03.021.

Schulz, M., Mudelsee, M., 2002. REDFIT: estimating red-noise spectra directly from unevenly spaced paleoclimatic time series. Computers & Geosciences, 28(3), 421-426. https://doi.org/10.1016/S0098-3004(01)00044-9.

Shen, M.M., Zan, J.B., Yan, M.D., Zhang, W.L., Fang, X.M., Zhang, D.W., Zhang, T., 2020. Comparative Rock Magnetic Study of Eocene Volcanogenic and Sedimentary Rocks From Yunnan, Southeastern Tibetan Plateau, and Its Geological Implications. Journal of Geophysical Research-Solid Earth, 125(2). https://doi.org/10.1029/2019jb017946.

Snowball, I.F., 1993. Geochemical control of magnetite dissolution in subarctic lake sediments and the implications for environmental magnetism. Journal of Quaternary Science, 8(4), 339-346. https://doi.org/10.1002/jqs.3390080405.

Su, Q.D., Nie, J.S., Luo, Z., Li, M.S., Heermance, R., Garzione, C., 2019. Detection of strong precession cycles from the late Pliocene sedimentary records of northeastern Tibetan Plateau. Geochemistry, Geophysics, Geosystems, 20(8), 3901-3912. https://doi.org/10.1029/2019GC008447.

Tabor, C.R., Otto-Bliesner, B.L., Brady, E.C., Nusbaumer, J., Zhu, J., Erb, M.P., Wong, T.E., Liu, Z.Y., Noone, D., 2018. Interpreting Precession-Driven δ18O Variability in the South Asian Monsoon Region. Journal of Geophysical Research: Atmospheres, 123(11), 5927-5946. https://doi.org/10.1029/2018JD028424.

https://doi.org/10.5194/egusphere-2026-2154
Preprint. Discussion started: 23 April 2026

Tan, M.Q., Zhang, W.L., Fang, X.M., Yan, M.D., Zan, J.B., Zhang, T., 2020. Rock magnetic record of core SG-3 since 1 Ma in the western Qaidam Basin and its paleoclimate implications for the NE Tibetan Platea. Palaeogeography Palaeoclimatology Palaeoecology, 560. https://doi.org/10.1016/j.palaeo.2020.109949.

Torrence, C., Compo, G.P., 1998. A practical guide to wavelet analysis. Bulletin of the American Meteorological society, 79(1), 61-78. https://doi.org/10.1175/1520-0477(1998)079%3C0061:APGTWA%3E2.0.CO;2.

Van Peer, T.E., Liebrand, D., Taylor, V.E., Brzelinski, S., Wolf, I., Bornemann, A., Friedrich, O., Bohaty, S.M., Xuan, C., Lippert, P.C. 2024. Eccentricity pacing and rapid termination of the early Antarctic ice ages. Nature Communications, 15(1), 10600. https://doi.org/10.1038/s41467-024-54186-1.

Wang, B., Biasutti, M., Byrne, M.P., Castro, C., Chang, C.P., Cook, K., Fu, R., Grimm, A.M., Ha, K.J., Hendon, H., 2021. Monsoons climate change assessment. Bulletin of the American Meteorological society, 102(1), E1-E19. https://doi.org/10.1175/BAMS-D-19-0335.1.

Wang, G., Wang, Y., Wei, Z., He, W., Zhang, T., Ma, X., 2020. Geochemical records of Qionghai Lake sediments in southwestern China linked to late Quaternary climate changes. Palaeogeography, Palaeoclimatology, Palaeoecology, 560: 109902. https://doi.org/10.1016/j.palaeo.2020.109902.

Wang, H.Y., Liu, W.G., Liu, Z.H., Qiang, X.K., Xu, X., Lei, J., Shi, Z.G., Cao, Y.N., Hu, J., Lu, F.Y., 2025. Pleistocene terrestrial warming trend in East Asia linked to Antarctic ice sheets growth. Nature Communications, 16(1), 8258. https://doi.org/10.1038/s41467-025-63331-3.

Wang, X.H., Wang, L.S., Hu, S.Y., Ma, M.M., Wang, Q., Cui, B.L., Zhan, C., Zeng, L., Liu, X.B., Shen, J., 2021. Indian summer monsoon variability over last 2000 years inferred from sediment magnetic characteristics in Lugu Lake, southwest China. Palaeogeography Palaeoclimatology Palaeoecology, 578, 110581. https://doi.org/10.1016/j.palaeo.2021.110581.

Wang, Y.J., Cheng, H., Edwards, R.L., Kong, X.G., Shao, X.H., Chen, S., Wu, J.Y., Jiang, X.Y., Wang, X.F., An, Z.S., 2008. Millennial- and orbital-scale changes in the East Asian monsoon over the past 224,000 years. Nature. https://doi.org/10.1038/nature06692.

Weedon, G. P., 2022. Problems with the current practice of spectral analysis in cyclostratigraphy: Avoiding false detection of regular cyclicity. Earth-Science Reviews, 235, 104261. https://doi.org/10.1016/j.earscirev.2022.104261.

Wen, Q., Liu, Z., Zhu, J., Yan, M., He, C., Han, J., Liu, J., Liang, Y., 2022. Local Insolation Drives Afro-Asian Monsoon at Orbital-Scale in Holocene. Geophysical Research Letters 49, e2021GL097661. https://doi.org/10.1029/2021GL097661.

Williamson, D., Jelinowska, A., Kissel, C., Tucholka, P., Gibert, E., Gasse, F., Massault, M., Taieb, M., Van Campo, E., Wieckowski, K., 1998. Mineral-magnetic proxies of erosion/oxidation cycles in tropical maar-lake sediments (Lake Tritrivakely, Madagascar): paleoenvironmental implications. Earth and Planetary Science Letters, 155(3-4), 205-219. https://doi.org/10.1016/S0012-821X(97)00217-3.

Wu, Z.P., Yin, Q.Z., Berger, A., Guo, Z.T., 2025. Forcing mechanisms of the half-precession cycle in the western equatorial Pacific temperature. Nat Commun, 16(1), 1841. https://doi.org/10.1038/s41467-025-57076-2.

https://doi.org/10.5194/egusphere-2026-2154
Preprint. Discussion started: 23 April 2026

Xiao, X.Y., Shen, J., Wang, S.M., Xiao, H.F., Tong, G.B., 2010. The variation of the southwest monsoon from the high resolution pollen record in Heqing Basin, Yunnan Province, China for the last 2.78Ma. Palaeogeography, Palaeoclimatology, Palaeoecology, 287(1), 45-57. https://doi.org/10.1016/j.palaeo.2010.01.013.

Xu, H., Liu, B., Wu, F., 2010. Spatial and temporal variations of Rb/Sr ratios of the bulk surface sediments in Lake Qinghai. Geochemical Transactions, 11(1), 3. https://doi.org/10.1186/1467-4866-11-3.

Xu, X.W., Qiang, X.K., Li, X.B., Qiu, H.J., Zhao, H., Fu, C.F., Yang, Z.Y., 2025. Magnetic proxy in the Heqing drill core revealed Indian Summer Monsoon variations linked with AMOC at the orbital -scale during the late Pleistocene. Palaeogeography, Palaeoclimatology, Palaeoecology 665, 112814. https://doi.org/10.1016/j.palaeo.2025.112814.

Xu, X.W., Qiang, X.K., Yang, Z.Y., Zhao, H., Fu, C.F., Wang, Q.Q., 2024. Magnetostratigraphy and relative paleointensity study of a late Quaternary lacustrine sediment sequence from Southwest China and its chronological significance. Palaeogeography, Palaeoclimatology, Palaeoecology. https://doi.org/10.1016/j.palaeo.2024.112067.

Xu, X.W., Qiang, X.K., Zhao, H., Fu, C.F., 2020. Magnetic mineral dissolution recorded in a lacustrine sequence from the Heqing Basin, SW China, and its relationship with changes in the Indian monsoon. Journal of Asian Earth Sciences 188. https://doi.org/10.1016/j.jseaes.2019.104081.

Yang, X.X., Jin, Z.D., Zhang, F., Ma, X.L., 2024. Glacial-interglacial lake hydrochemistry in step with the Pleistocene Indian summer monsoon at the southeastern Tibetan Plateau. Quaternary Science Reviews, 329, 108556. https://doi.org/10.1016/j.quascirev.2024.108556.

Zan, J.B., Kang, J., Yan, M.D., Fang, X., Li, X.M., Guan, C., Zhang, W.L., Fang, Y.H., 2018. A Pedogenic Model for the Magnetic Enhancement of Late Miocene Fluvial-Lacustrine Sediments From the Xining Basin, NE Tibetan Plateau. Journal of Geophysical Research-Solid Earth 123, 6176–6194. https://doi.org/10.1029/2018JB016064.

Zhang, C., 2020. Moisture sources for precipitation in Southwest China in summer and the changes during the extreme droughts of 2006 and 2011. Journal of Hydrology 591, 125333. https://doi.org/10.1016/j.jhydrol.2020.125333.

Zhang, J.H., Liu, B., Li, D.X., Zhou, X.H., Kang, X.L., Lin, Q., Wang, Y.H., Jiang, S., 2019. Magnetic Characteristics of Fluvial Deposit at the Baoji Section of the Weihe River and Its Response to Rainfall. Earth and Environment, 47(3), 235-245, https://doi.org/10.14050/j.cnki.1672-9250.2019.47.061.

Zhang, T.W., Yang, X.Q., Peng, J., Zhou, Q.X., Toney, J., Liu, H.Y., Xie, Y.X., 2023. Decoupled Indian summer monsoon intensity and effective moisture since the last glaciation in Southwest China. Geophysical Research Letters, 50(10), e2023GL103297. https://doi.org/10.1029/2023GL103297.

Zhang, W.L., Appel, E., Fang, X.M., Song, C.H., Cirpka, O., 2012. Magnetostratigraphy of deep drilling core SG-1 in the western Qaidam Basin (NE Tibetan Plateau) and its tectonic implications. Quaternary Research 78, 139–148. https://doi.org/10.1016/j.yqres.2012.03.011.

Zhang, Z.K., Liu, Z.Y., Li, G.J., Cai, Y.J., Wen, Q., Cheng, H., Lawrence Edwards, R., Lei, J., Liu, H., Jing, Z.W., 2025. Summer and nonsummer climatic signals in speleothem δ18O revealed by loess microcodium δ18O in East Asia. Proceedings of the National Academy of Sciences, 122(28), e2425565122. https://doi.org/10.1073/pnas.2425565122.

https://doi.org/10.5194/egusphere-2026-2154
Preprint. Discussion started: 23 April 2026

Zhao, C., Rohling, E.J., Liu, Z.Y., Yang, X.Q., Zhang, E.L., Cheng, J., Liu, Z.H., An, Z.S., Yang, X.D., Feng, X.P., 2021. Possible obliquity-forced warmth in southern Asia during the last glacial stage. Science Bulletin, 66(11), 1136-1145. https://doi.org/10.1016/j.scib.2020.11.016.

Zhong, W., Wei, Z., Shang, S., Ye, S., Tang, X., Zhu, C., Xue, J., Ouyang, J., Smol, J.P., 2018. A 15,400-year record of environmental magnetic variations in sub-alpine lake sediments from the western Nanling Mountains in South China: Implications for palaeoenvironmental changes. Journal of Asian Earth Sciences 154, 82–92. https://doi.org/10.1016/j.jseaes.2017.12.005.